Geophys. J. Int. (2000) **142,** 684–702

Shallow subduction zone earthquakes and their tsunamigenic potential

J. Polet and H. Kanamori
Seismological Laboratory, Caltech, Pasadena, CA 91125, *USA. E-mail: polet@gps.caltech.edu*

Accepted 2000 March 3. Received 2000 March 3; in original form 1999 August 16

SUMMARY

We have examined the source spectra of all shallow subduction zone earthquakes from 1992 to 1996 with moment magnitude 7.0 or greater, as well as some other interesting events, in the period range 1–20 s, by computing moment rate functions of teleseismic *P* waves. After comparing the source spectral characteristics of 'tsunami earthquakes' (earthquakes that are followed by tsunamis greater than would be expected from their moment magnitude) with regular events, we identified a subclass of this group: 'slow tsunami earthquakes'. This subclass consists of the 1992 Nicaragua, the 1994 Java and the February 1996 Peru earthquakes. We found that these events have an anomalously low energy release in the 1–20 s frequency band with respect to their moment magnitude, although their spectral drop-o is comparable to those of the other earthquakes. From an investigation of the centroid and body wave locations, it appears that most earthquakes in this study conformed to a simple model in which the earthquake nucleates in a zone of compacted and dehydrated sediments and ruptures up-dip until the stable sliding friction regime of unconsolidated sediments stops the propagation. Sediment-starved trenches, e.g. near Jalisco, can produce very shallow slip, because the fault material supports unstable sliding. The slow tsunami earthquakes also ruptured up-dip; however, their centroid is located unusually close to the trench axis. The subduction zones in which these events occurred all have a small accretionary prism and a thin layer of subducting sediment. Ocean surveys show that in these regions the ocean floor close to the trench is highly faulted. We suggest that the horst-and-graben structure of a rough subducting oceanic plate will cause contact zones with the overriding plate, making shallow earthquake nucleation and up-dip propagation to the ocean floor possible. The rupture partly propagates in sediments, making the earthquake source process slow. Two factors have to be considered in the high tsunami-generating potential of these events. First, the slip propagates to shallow depths in low-rigidity material, causing great deformation and displacement of a large volume of water. Second, the measured seismic moment may not represent the true earthquake displacement, because the elastic constants of the source region are not taken into account in the standard CMT determination.

Key words: earthquake, subduction, tsunami.

INTRODUCTION

In the last 10 years, several shallow subduction zone earthquakes have excited destructive tsunamis, causing more than 1500 casualties in the period 1992–1994 alone. In general, tsunamis are caused by large shallow earthquakes beneath the ocean floor. Thus, the size of the event is one of the most important parameters that determines its tsunamigenic potential. A great shallow earthquake beneath the ocean floor should always be expected to be followed by a substantial tsunami caused by the large displacement of water near the ocean floor. However, a subclass of shallow subduction zone earthquakes, 'tsunami earthquakes', poses a special problem.

A tsunami earthquake was originally defined as an earthquake that generates a tsunami larger than one would expect from its conventional magnitude (Kanamori 1972). Typical

examples are the 1896 Sanriku, Japan, and the 1946 Aleutian Island earthquakes. The source spectra of these tsunami earthquakes were more enhanced at long periods than ordinary earthquakes. Thus, when a moment magnitude scale, M_w, was introduced, a tsunami earthquake was generally identified as an event with a larger M_w than ordinary earthquakes with the same surface wave magnitude, M_S. Since surface wave magnitude is determined by the energy in surface waves with a period of 20 s and the moment magnitude measurement is based on longer periods for large events, this is an indication of the greater energy release in longer periods (or the 'slow' character) of these tsunami events. However, since M_S saturates, very large earthquakes with an ordinary source process tend to exhibit the same M_w–M_S disparity as tsunami earthquakes, which caused some confusion. Furthermore, some anomalously large tsunamis originate from a source other than a tectonic earthquake (i.e. faulting). Such sources include submarine or land slumping and volcanic activity. Also, in some cases, a tsunami can be amplified by focusing during propagation because of bathymetric features. In these cases, the causative earthquake itself is an ordinary event, but it exhibits the characteristic of a tsunami earthquake, namely a tsunami that is disproportionately large with respect to its moment magnitude.

Our primary interest in this paper is to examine shallow subduction zone earthquakes and their inherent tsunamigenic potential. Thus, we will focus our attention on a subset of tsunami earthquakes for which the large tsunami is due to an anomalous source faulting process. For these events, the development of a seismic discriminator for tsunami early warning purposes may be possible, whereas for the remainder an early warning system will probably have to involve a more direct approach, the measurement of water waves with pressure gauges, for example. In this paper we investigate the source spectra of shallow subduction zone earthquakes in a quantitative way, using broad-band teleseismic *P*-waveform recordings of worldwide seismic stations to determine the source spectra up to 1 Hz. We then compare these source spectra with the moment found by centroid moment tensor (CMT) inversion of very long-period surface waves. We will also discuss the mechanism, rupture direction, hypocentral location, tectonic setting and aftershock sequences of these earthquakes in an attempt to investigate more closely the origin of the tsunamigenic potential of these events.

A tsunami earthquake is usually described as having a long source time function and a slow and smooth rupture. Several explanations have been proposed concerning the more e cient (with respect to its M_S) tsunami-generating mechanism for these events, for example, the anomalously long source process time, which causes a large discrepancy between true seismic moment and conventional magnitude measurements made at shorter periods (Kanamori 1972), poor excitation of surface waves by nearly horizontal faults (Ward 1982) and more e cient excitation of tsunami waves by sources in sedimentary rocks than those in typical crustal rocks with the same seismic moment under specific geometries (Fukao 1979; Okal 1988).

Of particular interest here are five recent earthquakes that were followed by devastating tsunamis and have been termed tsunami earthquakes in previous studies: the 1992 Nicaragua event, the 1992 earthquake near Flores Island, the 1994 Java earthquake, the February 1996 event near the coast of Peru and the 1998 event near Papua New Guinea. The Nicaragua earthquake was the first tsunami earthquake to be captured by modern broad-band seismic networks, caused about 170 casualties and caused significant damage to the coastal areas of Nicaragua. In Flores, a 1992 field survey of the island showed that the first wave attacked the coast within five minutes at most of the surveyed villages. In total almost 2000 people were killed by the local tsunami, which reached as high as 26 m (Tsuji *et al.* 1995). The Java earthquake occurred o the southeastern coast of Java and generated a devastating tsunami that took the lives of more than 200 East Java coastal residents. Measured run-ups ranged from 1 to 14 m (Synolakis *et al.* 1995). The 1996 Peru earthquake struck approximately 130 km o the northern coastal region of Peru and created a tsunami that reached Peru, centred on the city of Chimbote (Bourgeois *et al.* 1999; International Survey Team 1997). We have also included the 1998 earthquake near New Guinea, which caused an even more destructive tsunami. Run-up heights for this event exceeded 10 m and thousands of people were killed.

METHOD AND DATA

In our analysis, we use teleseismic *P* waveforms recorded at worldwide broad-band stations, which we obtained from the IRIS Data Center. The method to determine the source spectra is described in detail in Houston & Kanamori (1986) and we will only briefly outline it here.

The moment rate (source) spectrum is given by

$$|\hat{M}(f)| = \frac{4\pi\rho\alpha^3 R_E \exp(\pi f t^*(\Delta))\hat{u}(f)}{g(\Delta)R_{\theta\phi}C|\hat{I}(f)|}, \quad (1)$$

where ρ and α are the density and *P*-wave velocity at the source, R_E is the radius of the Earth, $g(\Delta)$ is the geometrical spreading factor, $R_{\theta\phi}$ is the radiation pattern factor, C is the free surface receiver e ect, $t^*(\Delta)$ is the attenuation parameter, $\hat{I}(f)$ is the instrument response and $\hat{u}(f)$ is the spectrum of the observed *P* waveform.

We correct for station response (usually only the gain needs to be considered because of the broad-band nature of the stations) and for attenuation with a distance-dependent t^*, with $t^* = 0.7$ at 50°. The correction for the radiation pattern is applied to *P*, *pP* and *sP* phases, but since these three phases are usually di cult to separate for shallow large earthquakes, the correction is applied to the combined phases following the method of Boore & Boatwright (1984) and Houston & Kanamori (1986). The receiver site correction is computed for *P*-wave incidence at the free surface. These corrections are appropriate only at shorter periods (e.g. shorter than around 20 s). At the long-period end, we will use the seismic moment we determined by a centroid moment tensor inversion, which uses very long-period (3–7.5 mHz) surface wave data. To obtain the average moment rate function of the event, we average the corrected spectra in a logarithmic sense and obtain the standard deviation.

We examined the moment rate spectra for 38 shallow subduction zone events with moment magnitude greater than 7.0 (initially Harvard CMT moments were used in the selection process) in the time period 1992–1997 (Table 1 and Fig. 1) and added some other interesting/unusual events that occurred during the course of our study. Most of these earthquakes were thrust events, but several had a normal mechanism and

Table 1. Table of events used in this study.

No.	Origin time	CMT depth km	Centroid time s	CMT moment dyne cm	CMT latitude	CMT longitude	Strike	Dip	Slip	Event	ISC/PDE latitude	ISC/PDE longitude
1	920515070502	36	11	8.2e26	−6.15	147.19	275	42	77	New_Guinea	−6.053	147.633
2	920902001600	26	52	2.3e27	11.34	−87.58	132	70	94	Nicaragua	11.698	−87.402
3	921018151201	20	−2	7.6e26	6.97	−75.82	209	80	72	Colombia	7.110	−76.634
4	921212052927	20	21	5.2e27	−8.43	122.38	91	41	118	Flores	−8.543	121.864
5	930608130332	44	23	2.0e27	50.73	158.08	37	58	96	Kamchatka	51.165	157.763
6	930712131715	15	19	4.9e27	42.22	139.34	156	58	57	Sea_of_Japan	42.925	139.267
7	930910191254	21	13	6.0e26	14.02	−92.46	108	69	81	Chiapas	14.800	−92.687
8	940602181737	15	42	7.7e27	−11.44	113.02	98	85	90	Java	−10.539	112.849
9	941004132258	49	22	2.7e28	43.20	147.50	50	73	121	Kuril_1	43.756	147.256
10	941009075539	37	5	6.4e26	43.18	148.00	30	66	89	Kuril_2	43.952	147.878
11	941228121924	33	32	2.6e27	40.36	143.04	9	75	89	Honshu	40.536	143.415
12	950205225107	25	3	5.6e26	−37.79	178.72	206	30	−126	New_Zealand	−37.706	178.861
13	950505035346	28	11	2.7e26	12.67	125.72	352	70	97	Samar_1	12.681	125.244
14	950516201245	23	15	3.6e27	−22.73	169.67	133	60	−66	Loyalty	−22.982	170.010
15	950703195050	33	11	6.3e26	−29.30	−177.41	19	72	88	Kermadec	−29.459	−177.459
16	950730051121	31	32	1.2e28	−24.02	−70.37	355	25	85	Chile	−23.331	−70.307
17	950816102728	40	35	4.6e27	−4.99	153.65	331	54	104	Solomon_1	−5.757	154.302
18	950816231027	50	25	1.0e27	−6.22	155.46	126	31	80	Solomon_2	−5.757	154.416
19	950914140431	21	14	1.7e27	16.36	−98.48	120	79	92	Guerrero_1	16.752	−98.667
20	951009153551	33	36	7.5e27	18.58	−104.46	115	71	95	Jalisco	18.993	−104.245
21	951018103726	20	7	4.3e26	27.90	130.28	227	62	−61	Ryuku	28.041	130.237
22	951203180109	32	23	4.5e27	44.43	149.81	43	64	90	Kuril_3	44.669	149.277
23	960101080511	21	7	2.8e27	0.63	119.85	237	76	90	Sulawesi	0.68	119.81
24	960207213644	43	10	5.6e26	44.81	150.25	32	63	79	Kuril_4	45.32	149.91
25	960217055933	13	26	2.5e28	−0.70	136.18	122	8	109	Irian_Jaya	−0.95	137.03
26	960221125104	22	23	1.7e27	−10.09	−79.71	330	21	66	Peru_1	−9.62	−79.57
27	960225030816	13	13	8.7e26	15.35	−97.58	114	80	92	Oaxaca	16.20	−97.96
28	960610040334	33	23	3.6e27	50.27	−177.59	67	70	89	Aleutians	51.56	−177.63
29	960611182255	29	7	4.4e26	12.76	125.42	339	70	91	Samar_2	12.61	125.15
30	961002094801	32	9	5.6e25	11.94	126.26	355	70	92	Samar_3	11.76	125.48
31	961018105024	34	4	0.9e26	30.02	131.56	37	71	92	Kyushu_1	30.57	131.09
32	961019144442	30	1	1.0e26	31.61	132.20	27	63	86	Kyushu_2	31.89	131.47
33	961112165943	43	31	3.5e27	−14.71	−75.37	173	58	113	Peru_2	−14.99	−75.68
34	970326020857	30	11	1.1e26	50.60	179.55	60	63	78	Rat_Islands	51.28	179.53
35	970719142204	18	18	0.9e26	15.50	−98.18	95	69	82	Guerrero_2	16.33	−98.22
36	980717084915	15	18	4.3e26	−2.4	141.64	150	17	132	PNG	−2.96	141.93

less shallowly dipping reverse mechanisms. We limited the time period of our investigation to start after the Nicaragua earthquake of 1992.

As an illustration of our method, we present the results for the 1994 June 2 event that occurred south of Java, Indonesia. This event caused hardly any damage due to ground shaking, but excited a devastating tsunami. Data were available from more than 20 broad-band seismic stations from the IRIS Data Center in a suitable distance range (30–100°). The azimuthal and distance coverage as well as the data quality for this event were very good (Fig. 2). The source spectra for the di erent stations agree very well (a sample is shown in Fig. 3a), and we obtained the averaged moment rate spectrum shown in Fig. 3(b). As these figures show, after the corrections described in eq. (1) only minor variations of source spectrum with azimuth remain. Some of this may be due to directivity e ects (especially for larger earthquakes), and in some cases there is a local station contribution. We checked all the single-station spectra and removed those that were in clear error because, for example, of an incorrect gain or interference with another event. We can clearly see from Fig. 3(b) that the moment rate spectrum and total CMT moment of the Java event cannot be fitted by a standard ω^2 model, as shown by the grey reference lines. In the ω^2 model the moment rate function can be expressed as

$$\dot{M}(f) = \frac{M_0 f_0^2}{(f^2 + f_0^2)}. \tag{2}$$

Here f_0 represents the corner frequency, which can be expressed as

$$f_0 = c\beta\left(\frac{\Delta\sigma}{M_0}\right)^{1/3}. \tag{3}$$

The particular form of the moment rate spectrum (2) is not important. We use (2) simply as a reference spectrum and a guide for comparison of the observed source spectra for di erent events. Here β represents the shear wave velocity near the source, taken to be 3.75 km s^{-1} in the calculation of the reference curves and $c = 0.49$. The parameter $\Delta\sigma$ should be considered simply as a scaling parameter, rather than a specific source parameter. In this sense, we call $\Delta\sigma$ a stress parameter,

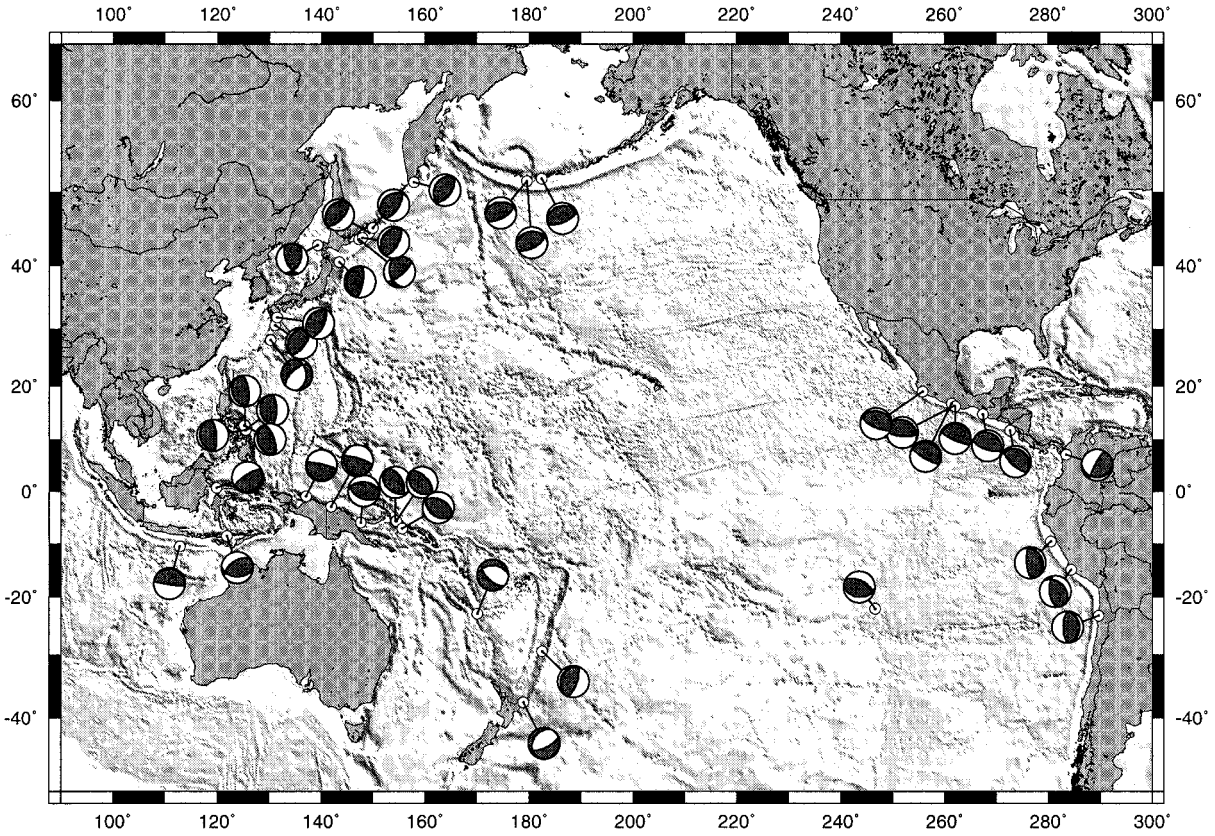

Figure 1. Earthquakes examined in this study. Focal mechanisms shown were computed using the CMT inversion of very long-period surface waves.

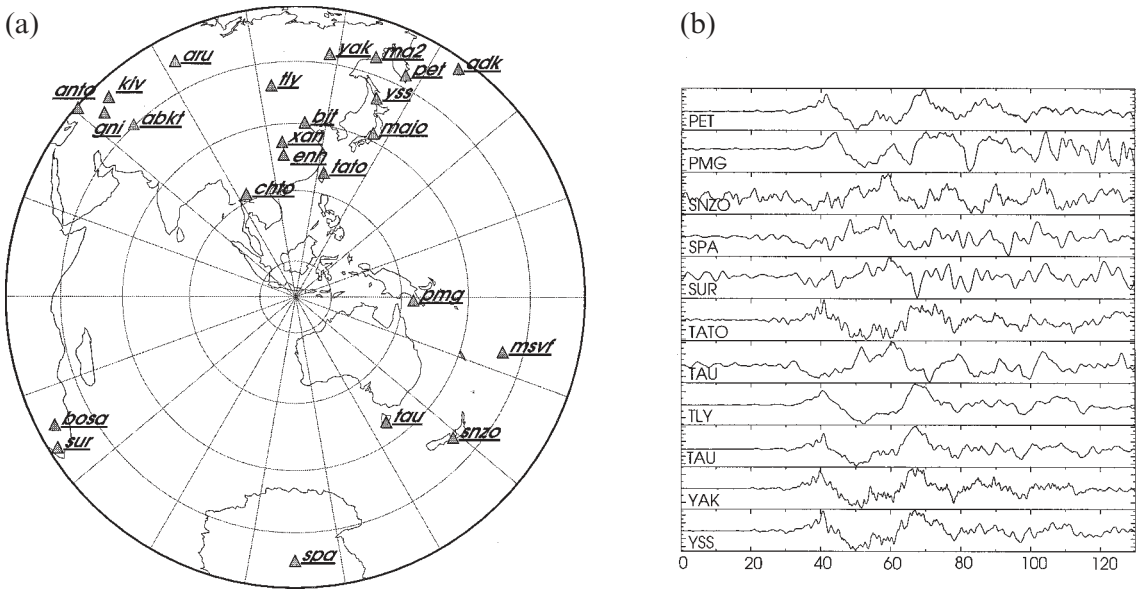

Figure 2. (a) Event and station locations for the 1994 Java event. (b) Examples of *P*-wave data used for this event, aligned on the predicted IASPEI91 traveltime.

following Boore & Boatwright (1984). The 'misfit' of the data to the reference model can be the result of many di erent factors, one obvious problem being the constants we have to choose in (1) and (2) (e.g. density and *S*-wave velocity near the source, as well as the stress parameter). To minimize this problem, we compare moment rate spectra for di erent events.

RESULTS: SOURCE SPECTRAL CHARACTERISTICS

To facilitate direct comparison of the di erent events, we plot the moment rate spectrum at four di erent frequencies (2, 5, 10 and 22 s) as a function of the total moment as determined

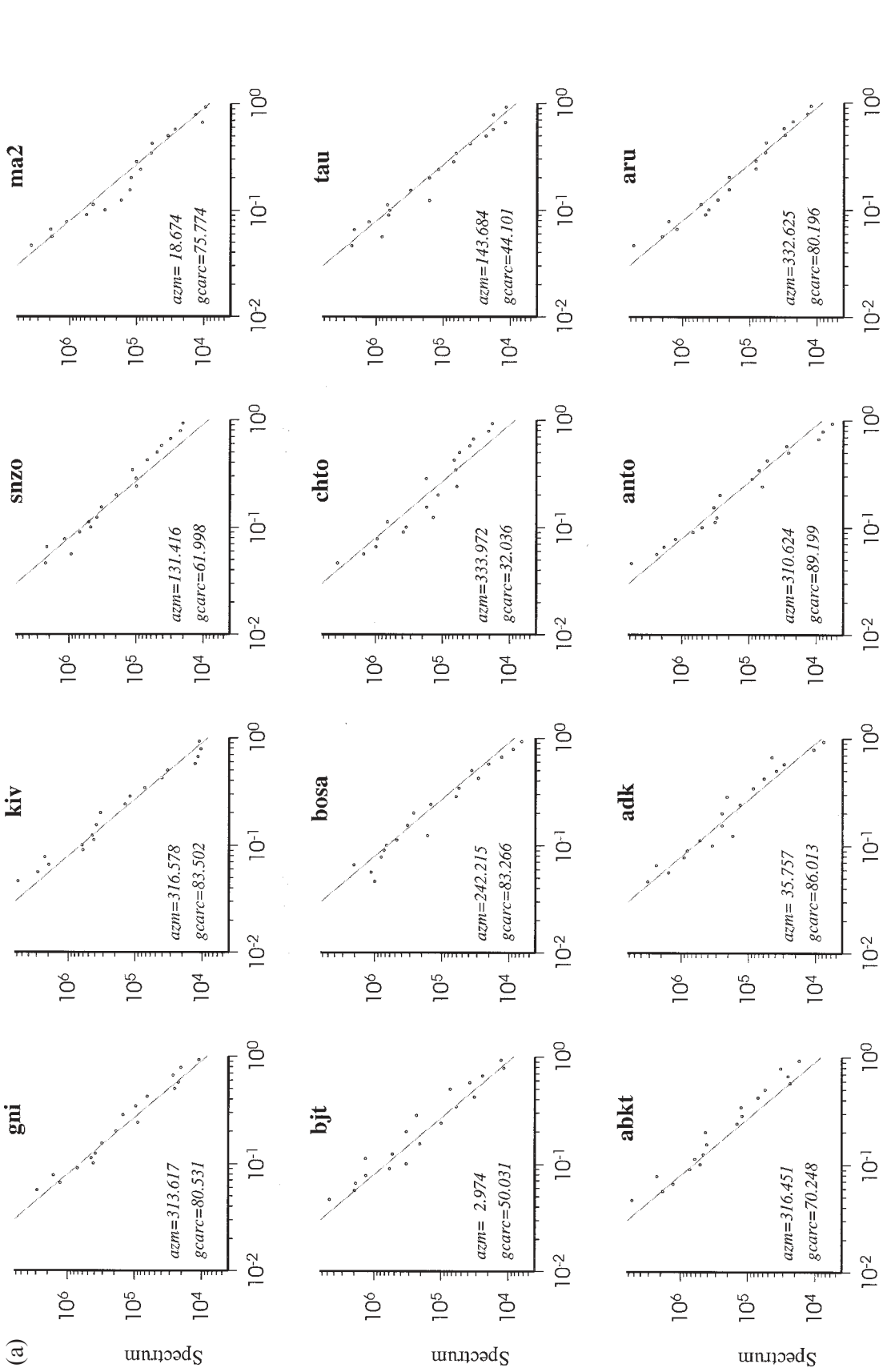

Figure 3. (a) Sample of moment rate spectra determined from *P*-wave recordings for the 1994 Java earthquake. (b) Averaged moment rate spectrum for the 1994 Java earthquake. The star indicates the CMT moment determined in this study and the triangle shows the Harvard CMT moment. Grey reference curves are calculated for an ω^2 model with a stress drop of 30 bar and an *S*-wave velocity of 3.75 km s^{-1}.

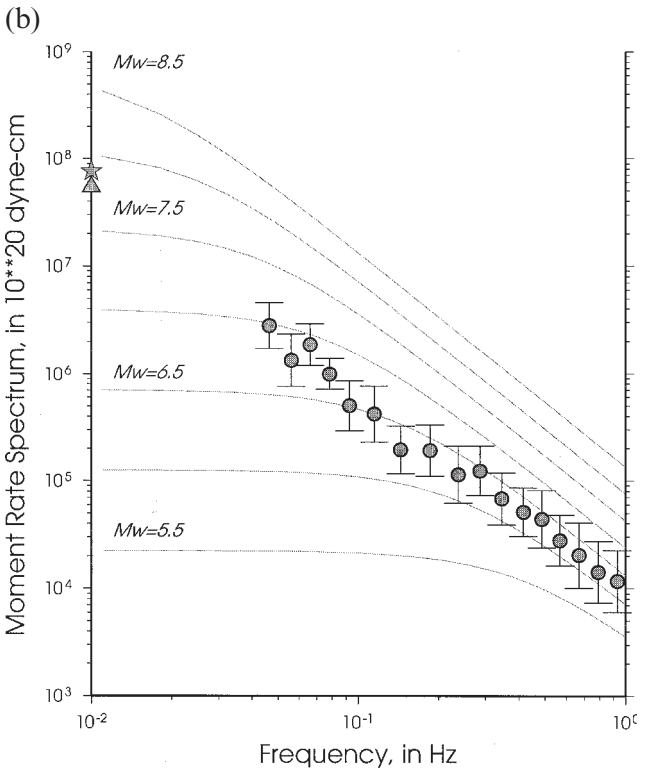

Figure 3. (*Continued.*)

in the CMT inversion for all events in Fig. 4 (moment rate functions for all analysed events can be found in Appendix A). As a reference, we again plot curves computed for an ω^2 model, for di erent stress parameters, which are shown by the numbers to the right of the corresponding grey curves. We also plot the 'average' energy release for all four periods in Fig. 5. These values correspond to the average of the log value of the moment rate at these four frequencies, or $(\log M_{22} + \log M_{10} + \log M_5 + \log M_2)/4$.

The five earthquakes that are of particular interest, because of the anomalously high excitation of tsunamis, are the Java, Nicaragua, Flores, Peru_1 and New Guinea events, which are marked by the numbers 8, 2, 4, 26, 36 and closed black circles. Of this group of tsunami earthquakes, the 1992 Flores event and the 1998 New Guinea event do not show 'anomalous' behaviour of the moment rate function; that is, these earthquakes have an average release of energy for all periods as a function of its total moment (Figs 4 and 5). This observation for the Flores event is consistent with the hypothesis that the tsunami following this earthquake was not directly caused by the earthquake itself, but was an e ect of landslides triggered by the quake (Tsuji *et al.* 1995; Hidayat *et al.* 1995). The evidence for this is in the observation of collapsed cli faces and landslides on the island itself and its neighbouring islands. Our results for the New Guinea event suggest that the origin of its unusual tsunami excitation is more likely to be related to local bathymetric e ects, or a landslide, and is probably not associated with the source character of the earthquake itself, which is confirmed by early results from other studies implying that a sediment slump may be the cause (Tappin *et al.* 1999). The other three events in this group of five tsunami earthquakes, however, all show a low-energy release at shorter periods with respect to their total moment as measured at longer periods or 'a small stress parameter' (Fig. 5) and could be called 'slow' earthquakes. These results agree with the energy analysis of Newman & Okal (1998). In the case of Nicaragua and Java, this deficiency in energy is consistent for all periods shown in Fig. 4; for the Peru_1 event this is less pronounced at the shorter periods, but is obvious for moment release at a period of 22 s (this may be caused by the relatively poor data for this event).

In Fig. 5 we have thus identified a subclass of tsunami earthquakes, namely the group of slow tsunami earthquakes, that includes the Peru_1, Nicaragua and Java events. The anomalous tsunami excitation for this group seems to be directly related to the slow character of the earthquake source, since no related process such as a landslide, for example, has been identified as being the cause. Also of interest is the comparison between Peru_1 (#26) and Peru_2 (#33). These two events were located close to the coast of Peru, but show clearly di erent frequency contents. As we can see from Fig. 5, our analysis can be used as an accurate discriminant for slow tsunami earthquakes, and could be available within hours of an event, making it possible to release a tsunami warning in time for the teleseismic arrival of the water waves.

Another parameter in our analysis is the value of spectral drop-o . To determine this value, we fit the moment rate values (not including the CMT moment) by a curve of the form

$$\dot{M}(f) = \frac{M_0 f_0^n}{f^n + f_0^n}, \tag{4}$$

where n represents the spectral drop-o . In general, the value of M_0 was poorly constrained by this fit because for most events the corner frequency was not reached within the measured frequency window, making the abscissa di cult to predict. However, the value for n (spectral drop-o) was generally well determined. We have plotted the values for spectral drop-o thus obtained for all earthquakes in Table 1 in Fig. 6.

The Nicaragua, Java and Peru_1 events, which were previously identified as having an anomalously low energy release at higher frequencies, do not show any evidence for an anomalous value of spectral drop-o . In fact, these events are located very close to the median value for all shallow subduction zone earthquakes. This indicates that the energy release is consistently low for the examined frequency band, and there is no general di erence in the spectral drop-o between tsunami earthquakes and regular earthquakes. In general, the drop-o values for all examined shallow subduction zone events lie between 1.25 and 2.60, with an average value of 1.8, demonstrating that an ω^2 approximation is fairly appropriate for most events. From Fig. 6 there also seems to be a regional trend in the spectral drop-o values; for example, the events in the Central American subduction zone (2, 7, 19, 20, 27) tend to have a relatively rapid drop-o , and the values for events in the Kurils (9, 10, 22, 24) are all close to 1.6.

Another parameter of interest for tsunami earthquakes is the source duration. In our CMT inversion the centroid time gives a value comparable to half of the source duration. Although the resolution of this calculation is not high for such long-period surface waves (3–7.5 mHz), and will also be influenced by errors in origin time and location, it can still give a good indication of anomalous behaviour of an event. In Fig. 7 we

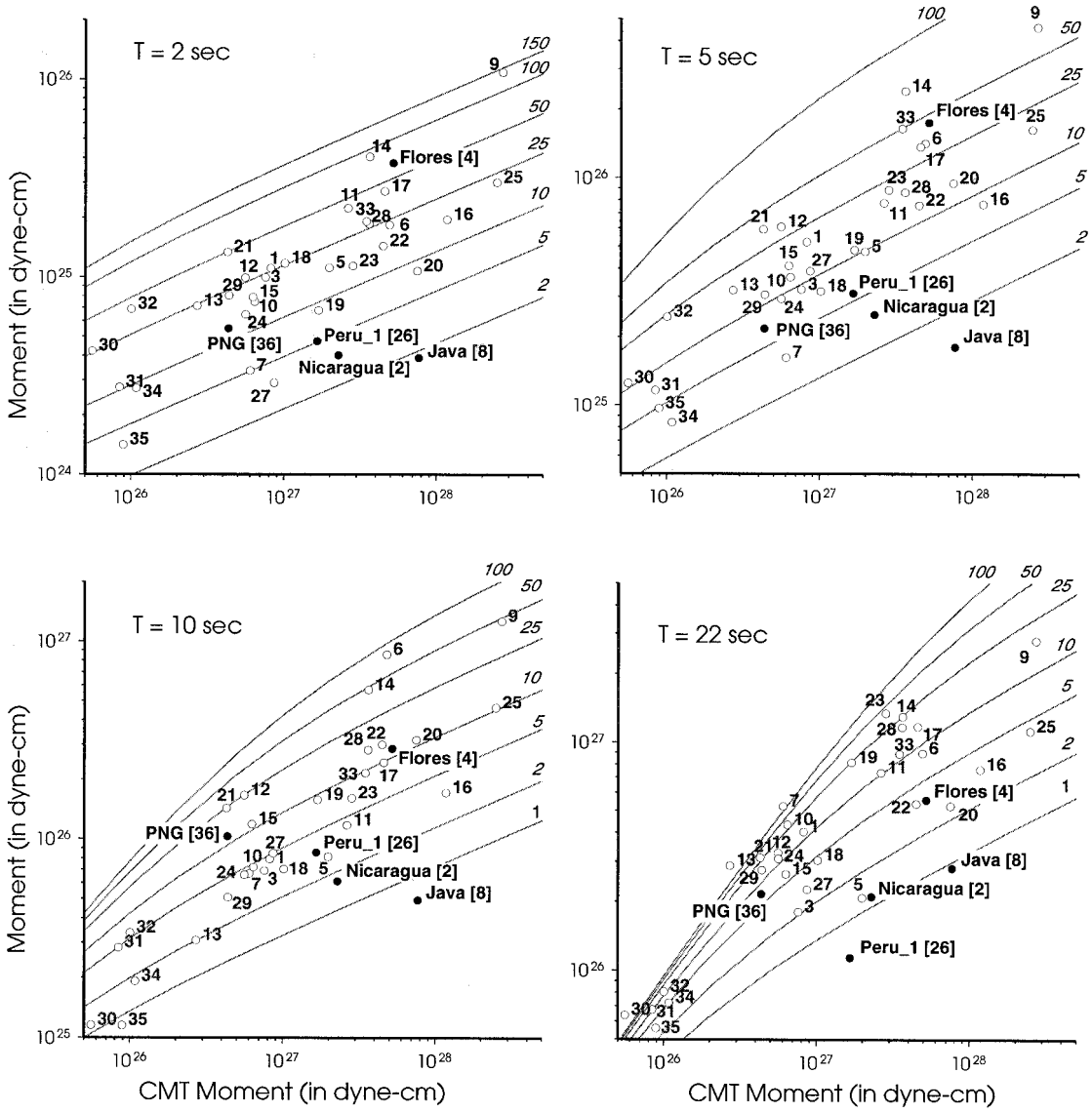

Figure 4. Moment rate values for the chosen periods (2, 5, 10, 22 s) as a function of total moment as determined by CMT inversion of long-period surface waves. Reference curves were calculated for an ω^2 model. Values next to the grey curves indicate the stress drop used to calculate the reference curve. Event numbers (Table 1) are given next to the corresponding moment rate values. Tsunami earthquakes are indicated with closed circles.

have plotted the centroid time minus origin time as a function of total moment. Although there is a large scatter in values, we can see a clear correlation of total moment with source duration, as is expected from the standard scaling relationships. For reference, we show the line $\log M \approx 3 \log \tau$, and this relation seems to be appropriate for this data set. Also obvious is the long source duration of both the Nicaragua and the Java events. An approximately 100 s source duration for the Nicaragua event has been found by many previous studies (e.g. Kanamori & Kikuchi 1993; Imamura *et al.* 1993; Ide *et al.* 1993 and Ihmle 1996). The Peru_1 event, however, does not have an anomalously long source time function.

Since slow tsunami earthquakes have both a relatively long source duration and a low energy release in the 20 s range, an anomalously high ratio of these two values (duration/energy) could be used as an indicator of a high tsunami-generating potential of an event, and thus serve as a fast discriminant.

PROXIMITY TO TRENCH AND RUPTURE DIRECTION

To examine the event location and rupture direction, we plotted the centroid location from both our and Harvard's inversions, and the ISC/PDE location on maps of seafloor topography. Ship soundings constrain the long-wavelength bathymetry and Geosat–ERS-1 gravity anomalies constrain the short-wavelength bathymetry (Smith & Sandwell 1997). We consider that the Harvard CMT location is the more accurate of the two because of its use of shorter-period (45–135 s) waves and application of tomographic models for phase corrections. For some events there are fairly big di erences in the two CMT locations. This may be partly due to a true physical di erence in the centroid location of long-period versus shorter-period energy, but we believe it is largely due to the lack of a well-defined maximum in variance reduction for

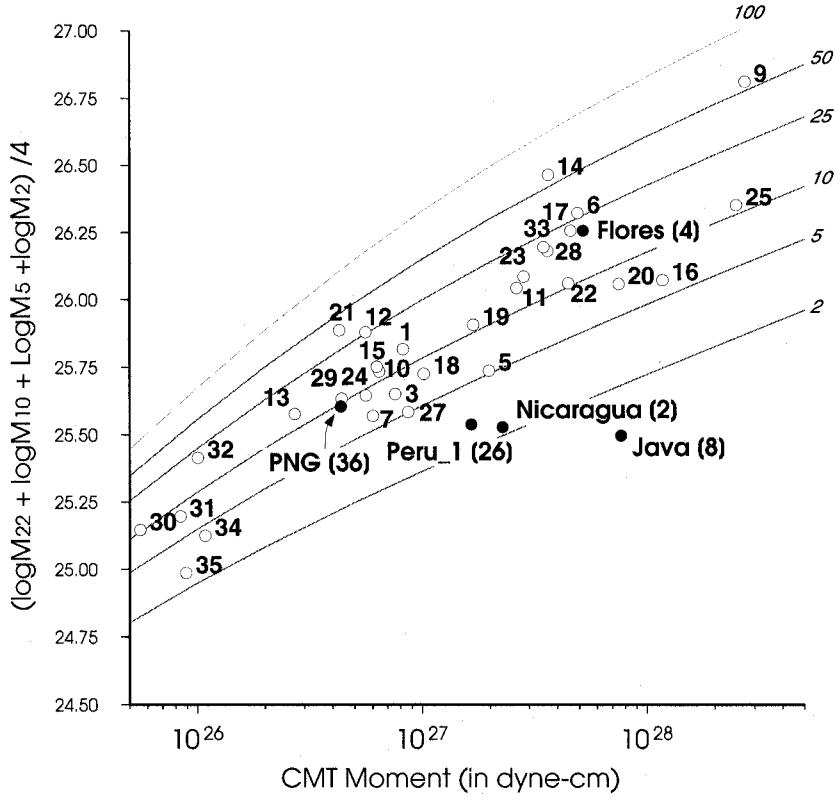

Figure 5. Average log value for moment rate for four periods (2, 5, 10, 22 s). Annotation is as in Fig. 4.

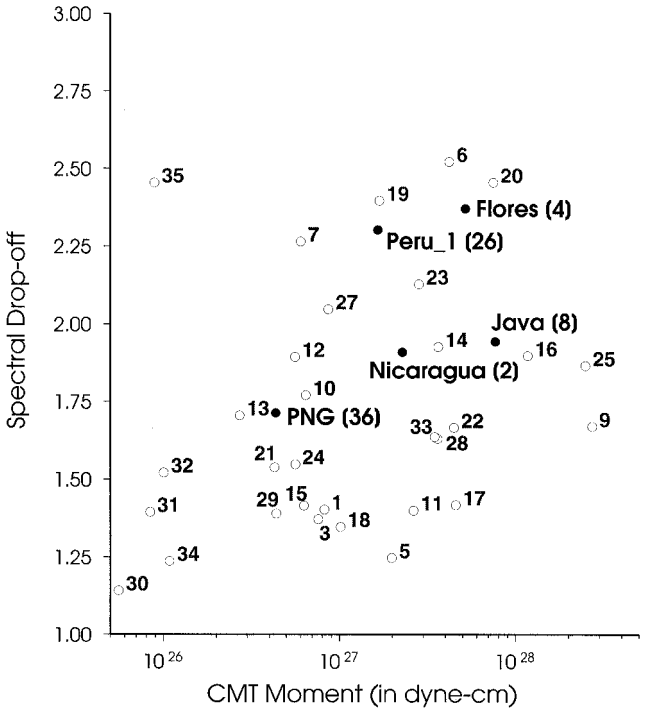

Figure 6. Spectral drop-o values as a function of CMT total moment determined by fitting the measured moment rate values by a function of the form of eq. (3).

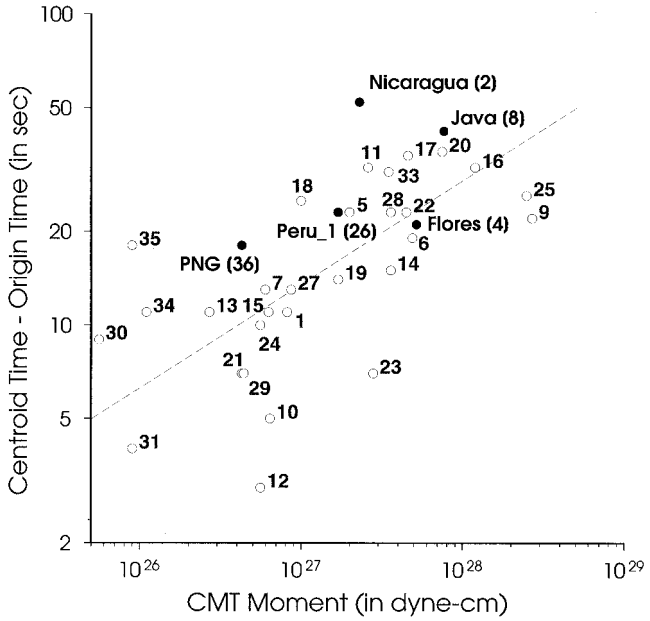

Figure 7. Centroid time as determined by long-period CMT inversion minus origin time plotted as a function of CMT moment. The dashed reference line has slope of power 3, indicating a log $M \approx 3 \log \tau$ relation.

the long-period surface waves. When available we used the relocated ISC hypocentre data (Engdahl *et al.* 1998), and for more recent events we used the PDE event location.

Fig. 8 shows one of these maps for the Central American subduction zone and includes the locations of six earthquakes that were investigated in this study. Since the ISC location is

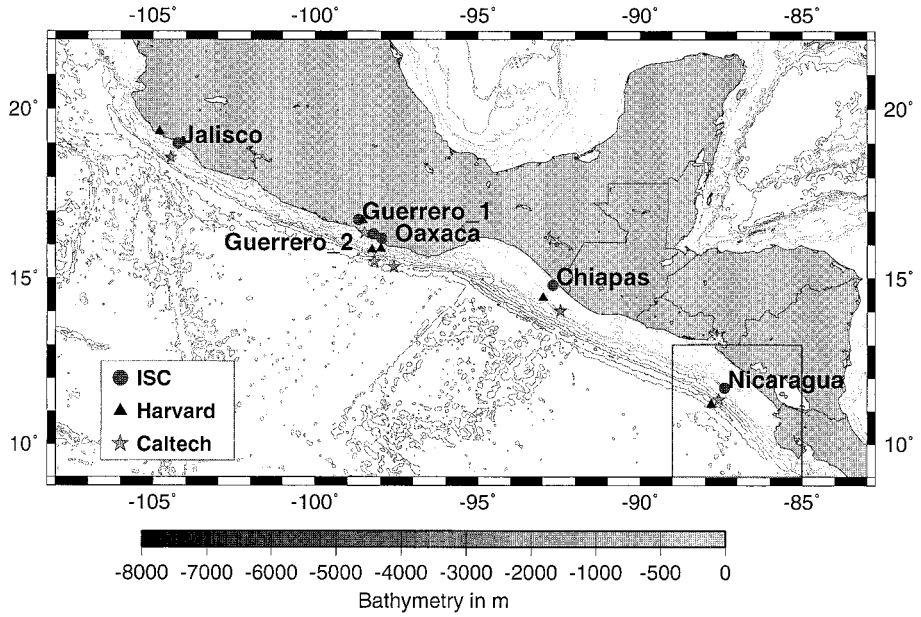

Figure 8. Map of the Central American subduction zone with contours of seafloor topography in metres from Smith & Sandwell (1997). Circles denote the ISC/PDE epicentre, stars show the centroid as determined in this study and triangles represent the Harvard centroid location. Box shows area enlarged in Fig. 10(a).

determined using short-period body waves (mostly direct *P* and *S* waves), we interpret this location as representative of the start of the rupture. The centroid locations, measured at longer periods, show the centroid of moment release. The direction from the ISC to the centroid location indicates the rupture direction of the events.

As can be seen from Fig. 8, all earthquakes in this region ruptured trenchwards, with the centroids for Guerrero_2 and Nicaragua located close to the axis of the trench. The same two events were depleted in high-frequency energy (numbers 35 and 2 in Fig. 5), although the moment of the Guerrero event was probably too small to generate a sizeable tsunami. There is also some indication of the Jalisco and Oaxaca centroids being near the trench, but the two centroids do not agree here. Work by Pacheco *et al.* (1997) indicates that the Jalisco earthquake ruptured unusually close to the trench, but has an overall NW directivity. Fig. 9 shows similar maps for the South American and Java trenches and the events in these regions. Again, the tsunami earthquakes (Peru_1 and Java) both ruptured up-dip and their final centroids were located close to the trench. The other events in these figures clearly do not rupture as close to the deepest part of the trench. Another interesting observation is that all three tsunami events studied in this paper were located in areas where the trench is far removed from the coastline.

Most earthquakes in Table 1 were determined to have ruptured up-dip or trench-parallel, or the locations were too close to each other to give a clear indication of rupture direction. The one exception is the Honshu event (number 11 in Table 1) of December 1994, which clearly ruptured in the down-dip direction, as confirmed by other studies (Hartog & Schwartz 1996; Nakayama & Takeo 1997; Sato *et al.* 1996; Tanioka *et al.* 1996). In conclusion, the three tsunami earthquakes showed a relatively strong directivity and their centroids were all located unusually close to (basically in) the deepest part of the trench compared to the 'normal' events. The shallow depth of these events can be related to the slow character that was demonstrated in the previous section of this paper through the observation of Bilek & Lay (1999) that there is a systematic decrease in source duration with increasing depth along the subduction zone interface, which they attributed to variations in sediment properties on the plate contact. Also, the distance from the trench where the events occurred to the coastline is unusually large.

AFTERSHOCK SEQUENCE

In addition to the location of the centroids, these slow tsunami earthquakes seem to have another remarkable characteristic. In Fig. 10 we show the Harvard CMT aftershock mechanisms for the two largest tsunami earthquakes: the Nicaragua event (Fig. 10a) and the Java earthquake (Fig. 10b). Both of these events have a large number of normal fault aftershocks; for the Java earthquake, the clear majority of the aftershocks show a normal fault mechanism. In the case of the Nicaragua event the normal faulting events seem to be located in the outer rise region, judging from their centroid locations. This picture is not so clear for the Java aftershocks. The Peru_1 event is of much smaller magnitude and had only two aftershocks large enough to be included in the Harvard catalogue. One of these mechanisms was a shallow thrust and the other showed a normal faulting mechanism.

There are various possible explanations for the relatively great number of normal faulting aftershocks. Because the location of the tsunami events is very close to the trench axis itself, stress triggering of normal faulting events in the outer rise would be more likely than for 'normal' subduction events, which are located further landwards. Another explanation involves the generally aseismic nature of shallow subduction zones near the trench. Because of the proximity of the rupture zone of slow tsunami earthquakes to the trench, there are relatively few aftershocks with thrust mechanisms. This results

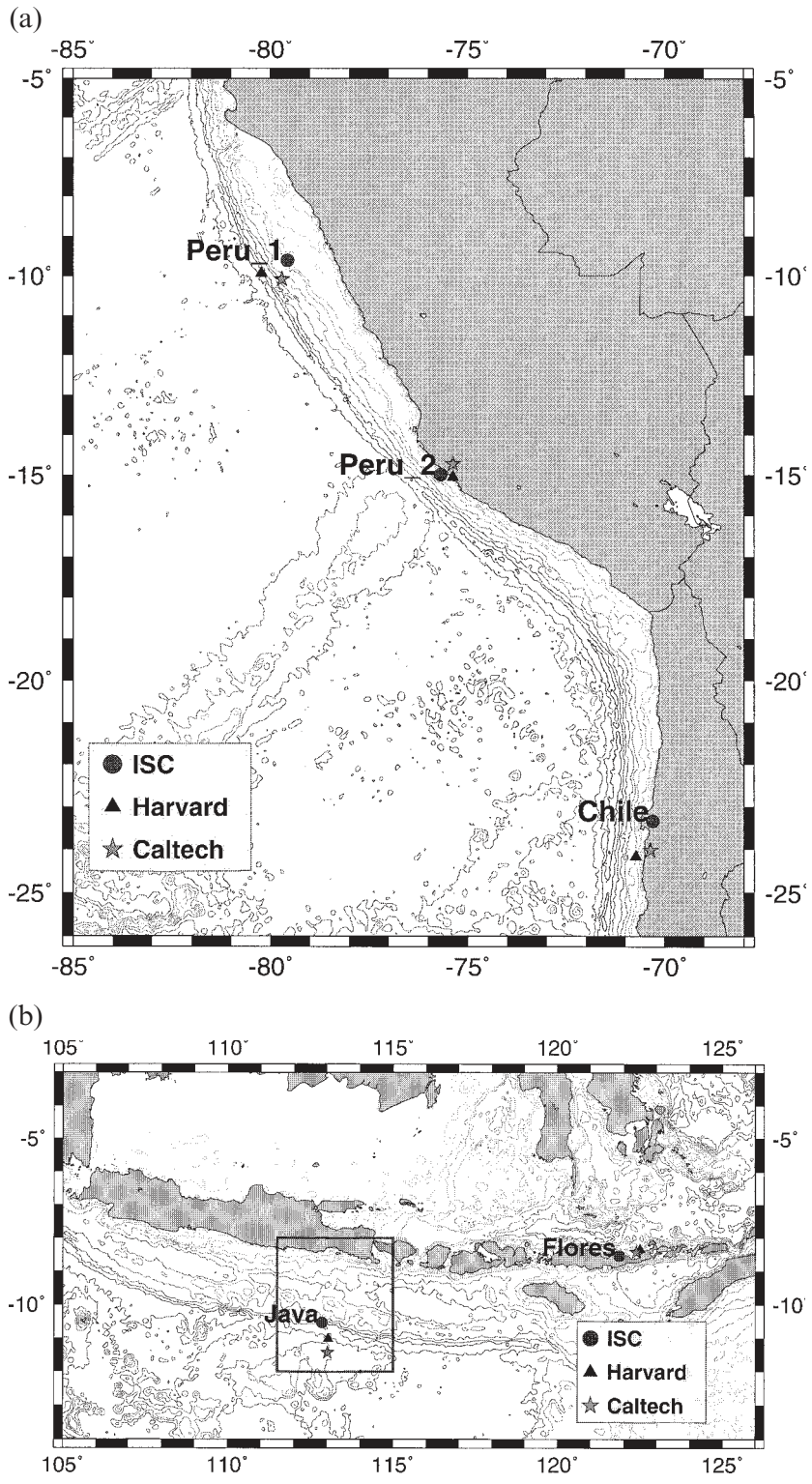

Figure 9. Contour maps of seafloor topography in metres for the South America (a) and Java (b) trenches. Symxbols as in Fig. 8. The box in (b) indicates the area shown in Fig. 10(b).

in an increase in the ratio of normal to thrust aftershocks. We will discuss this in more detail later in this paper. Alternatively, the main event may have triggered slumping events in the accretionary prism or forearc region, although the CMT depths of these events do not seem to be that shallow. Another possibility is that these events are related to the structure of the subducting plate, which, as we will show later in this paper, in these regions seems to be highly faulted into a horst-and-graben structure. Several modelling studies of stress alterations caused by large subduction earthquakes also suggest that, as a result of the subduction slip, the whole area towards the trench and outer rise experiences an increase in tensional

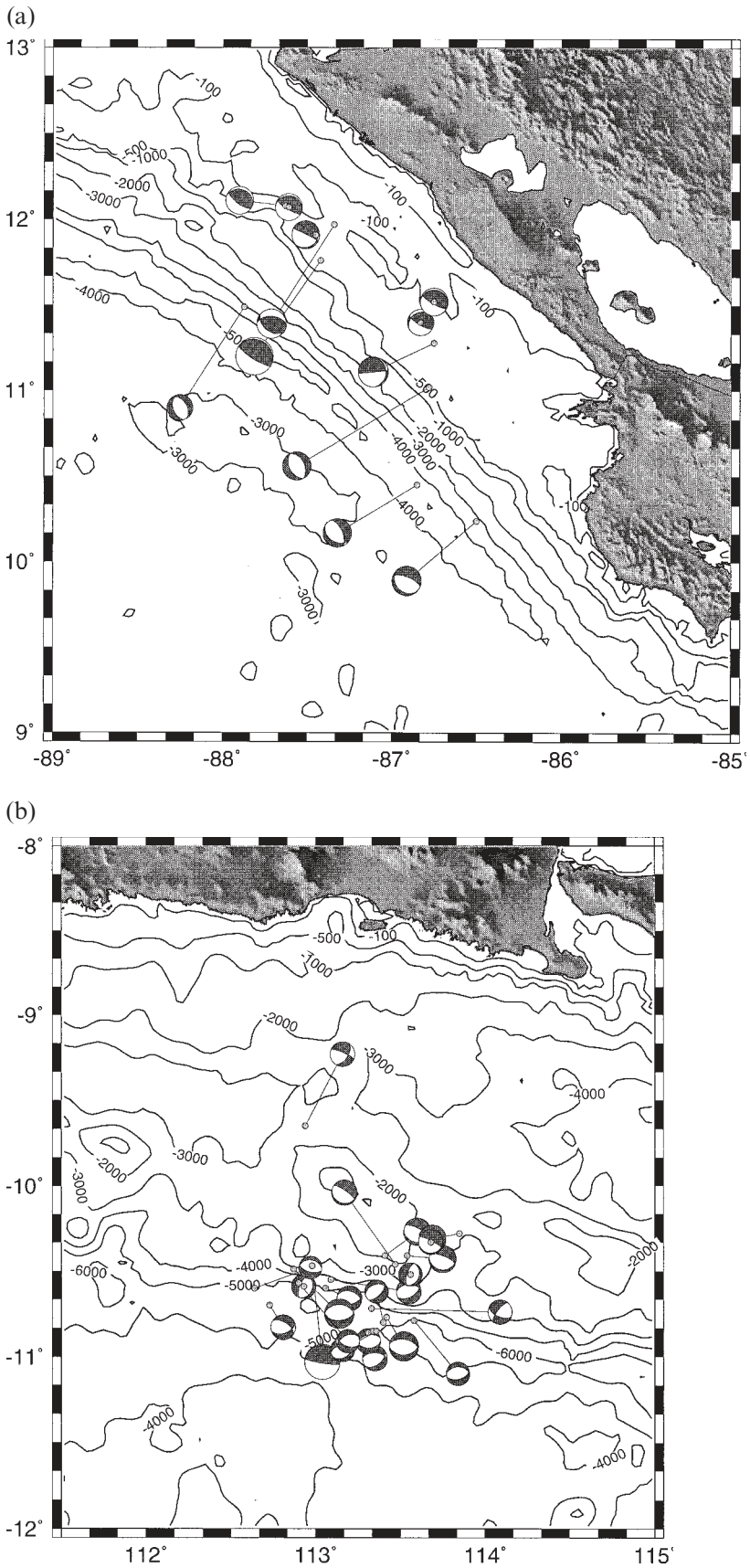

Figure 10. (a) Aftershock sequence of the Nicaragua earthquake. Harvard CMT solutions for a time period of 100 days after the main shock are shown, with the focal spheres plotted on the Harvard CMT location. Dotted lines connect the CMT locations to the original PDE locations. (b) Same for the Java event.

stresses, which would favour normal events in zones towards the ocean from the upper limit of the rupture (Taylor *et al.* 1996; Dmowska *et al.* 1996). More definite conclusions can only be drawn after a detailed investigation of the location, depth and source mechanisms of these aftershocks, which is beyond the scope of this paper, and will be the subject of a future paper.

SEDIMENT THICKNESS AND STRUCTURE OF THE SUBDUCTING PLATE

Because of the slow rupture of tsunami earthquakes, several researchers have suggested that sediments may play an important role in the tsunamigenic potential of these events (Okal 1988; Kanamori & Kikuchi 1992; Ihmle 1996; Tanioka *et al.* 1997). We obtained a global grid of sediment thickness from the National Geophysical Data Center (NGDC) to examine the relationship between tsunamigenic potential and sediment thickness more closely. However, this data set has significant inaccuracies and parts of it have been determined by extrapolation and interpolation, so conclusions based on this data set have to be tentative. To supplement this database we will use more local data sets, described in e.g. von Huene & Scholl (1991) and Hilde (1983).

The Nicaragua earthquake occurred near the Mid-American trench, on the subduction interface between the Cocos and North American plates. This area is located between the Costa Rica and Guatemala trenches, which are described as type 2 margins (Fig. 11) according to the classifications of convergent margins by von Huene & Scholl (1991). From the NGDC sediment thickness database, a small accretionary prism seems to be present locally near the centroid of the Nicaragua event, between two local minima in sediment thickness. The suggestion that this event occurred near a margin with only a small accretionary prism (< 5 km wide) and a thin sedimentary cover on the subducting oceanic crust is confirmed by the preliminary work of Walther & Flueh (1998), which was part of the PACOMAR 3 project. This project conducted a ship survey along the Pacific coast of Nicaragua in the spring of 1996. The resulting geophysical data set also shows slide scars at the edge of the shelf, which may have formed during tsunamigenic earthquakes, and a highly faulted oceanic crust adjacent to the trench (von Huene *et al.* 1998). This extensive horst-and-graben structure of the oceanic plate, which even cuts up the seamounts as the crust is flexed (von Huene, personal communication, 1999), provides a lot of space for sediments to subduct (Walther, personal communication, 1999).

Both the Peru and the Java continental margins near the centroid of the studied tsunami earthquakes are described as Type 1 margins by von Huene & Scholl (1991). The existence of only small accretionary prisms is confirmed by the sediment thickness maps of these regions and local studies of the area. Long-range sidescan sonar swath images of the Java trench show normal faults in the ocean floor near the trench, resulting from the tension related to the bending of the oceanic lithosphere into the subduction zone (Masson *et al.* 1990) and areas of small seamounts being subducted. There is evidence for a small accretionary prism and a thin subducting sedimentary section (Masson *et al.* 1991). Studies of the Peru margin near

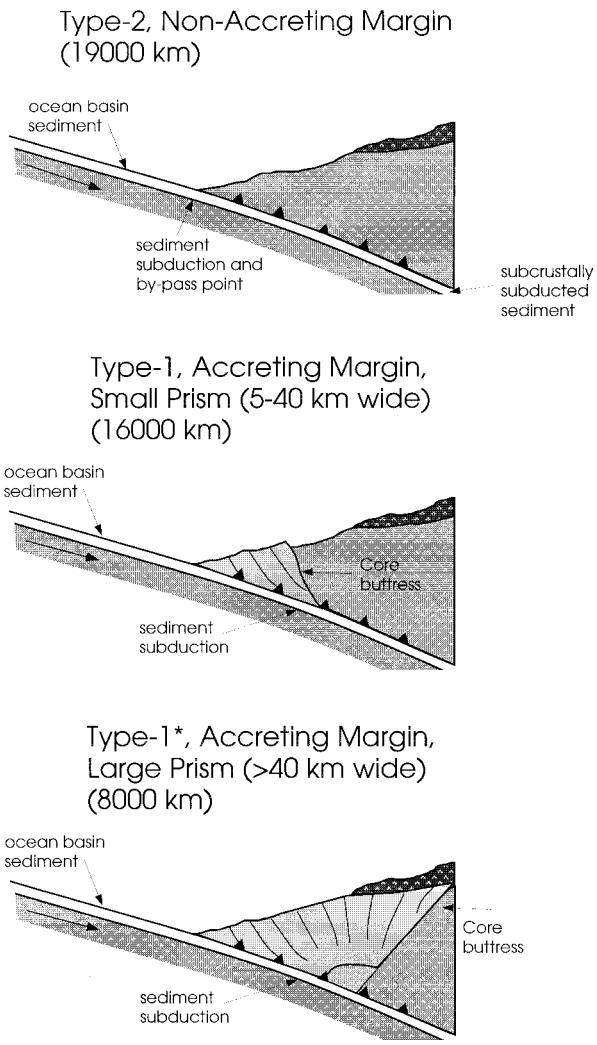

Figure 11. Simplified diagrams of three types of continental margins (adapted from von Huene & Scholl 1991): type 2 or non-accreting margins; type 1 margins with small to medium prisms; and type 1* margins with large accretionary prisms. The approximate global lengths of these margins are shown.

the 1996 tsunami event showed large subducted grabens containing trench deposits (Hilde 1983; Kulm *et al.* 1981). The trench has a small accretionary prism (13 km width) and a thin layer of subducting sediments (500 m) (von Huene *et al.* 1996). Studies to the south of this region show a highly developed horst-and-graben structure of the oceanic plate near the trench, possibly related to the subduction of the Nazca ridge.

INTERPRETATION

The tsunami earthquakes described in this paper seem to have several important factors in common:

(1) a long source duration (slow rupture velocity) with relatively low energy release at high frequencies;

(2) the rupture propagates up-dip to very shallow depths (or possibly even the ocean floor surface);

(3) the distance from the trench where the events occurred to the coastline is unusually large;

(4) a relatively high percentage of normal faulting aftershocks;
(5) a subducting sedimentary layer and only a small accretionary prism in the trench;
(6) the ocean floor near the trench is highly faulted, indicative of strong horst-and-graben structures in the subducting slab.

In general, shallow-dipping subduction zones with a relatively young (< 100 Ma) oceanic crust, where there exists strong coupling between the downgoing slab and the upper plate, can be described by the following model (Fig. 12). Earthquakes only nucleate over a limited depth range, which is called the seismogenic zone, and constitutes a frictionally unstable region. No nucleation takes place in the seaward up-dip portion and landwards down-dip of a critical point (e.g. Byrne *et al.* 1988; Hyndman *et al.* 1997; Scholz 1998). No earthquake can nucleate in the seaward shallow zone (which is commonly called 'aseismic') as a consequence of the presence of unconsolidated, granular sediments, which form a stable sliding (velocity strengthening) zone. In this zone, plate motion is accommodated in the form of creep. If earthquakes propagate into this stable region, a negative stress drop will occur, resulting in a rapid stop to the rupture propagation (Scholz 1998). The third frictional stability regime is the conditionally stable regime; earthquakes can propagate into such a region but no earthquake nucleation can take place.

The transition from the upper stable zone to the unstable zone, which marks the up-dip limit of the seismogenic zone, occurs when either the 'backstop' (or core buttress, see Fig. 12) is reached (that is, the thrust fault plane first contacts overlying continental or island arc crust) or the temperature reaches the dehydration temperature of the smectite–illite transition for smectite clays (100–150 °C), present in most accreted sediments. Illite clays may exhibit stick-slip behaviour after most free water is lost, whereas smectites will exhibit stable sliding even after most free water is expelled (Wang & Mao 1979).

Two di erent factors may determine the down-dip limit of the seismogenic zone. At some depth a temperature is reached on the fault where the rocks start to behave plastically, and this critical temperature is about 300–350 °C. Large earthquakes, initiated at less than this critical temperature, may still extend to a depth with a temperature of about 450 °C with conditional stability, but below this depth stable sliding behaviour takes over. An alternative down-dip limit could be the forearc mantle, where the presence of serpentinites exhibits conditionally stable behaviour (Hyndman *et al.* 1997).

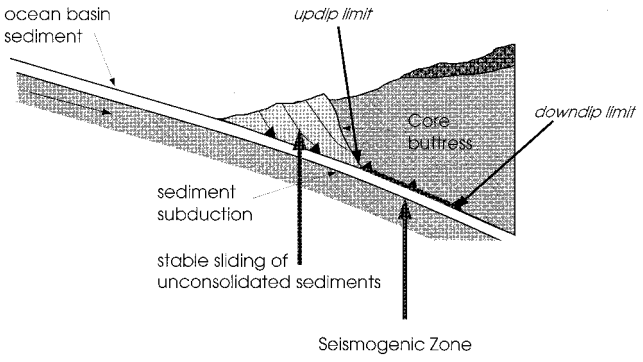

Figure 12. A simplified model of the seismogenic zone of subduction thrust faults. The seaward up-dip part of the fault exhibits stable sliding behaviour, as does the part of the fault that is down-dip of a critical point.

Most earthquakes examined in this study agree with this simple model. The events nucleate in the seismogenic zone at about 20 or 30 km depth, propagate up-dip through the conditionally stable region of compacted, dehydrated sediments, but cannot penetrate into unconsolidated sediments, where either stable sliding or creep-like volumetric deformation occurs. Thus, most earthquakes do not produce large shallow seafloor deformation and the volume displacement of water is not very large. As a result, no anomalously large tsunamis are generated by these events. Since the rupture does not propagate a long distance through sediments, these earthquakes are not slow. This could be termed a 'regular' shallow subduction zone earthquake.

The events analysed in this study have demonstrated that there are several exceptions to this simple model of shallow subduction earthquakes, where no or little very shallow slip occurs. The Jalisco earthquake, for example, did rupture close to the trench. However, this region of the middle American subduction zone seems to be depleted in sediments (Pacheco *et al.* 1997). This would make it possible for an earthquake to rupture all the way to the ocean floor surface, unhindered by stable sliding sediments (Fig. 13a). This is in contrast to the Nicaragua, Java and Peru earthquakes. These events also ruptured up to the trench although there are sediments being subducted. In these cases, an explanation may be found in the model that Tanioka *et al.* (1997) proposed for the Japan trench region. In all three regions, the ocean floor close to the trench was found to be highly faulted, suggesting that the subducting plate is rough and exhibits a well-developed horst-and-graben structure. As these structures are subducted with sediments in the graben part (but not covering the horsts), the horsts can create enough contact with the overriding block to cause an earthquake in the shallower part of the interface zone (Fig. 13b). Since there is only a small accretionary prism present near the

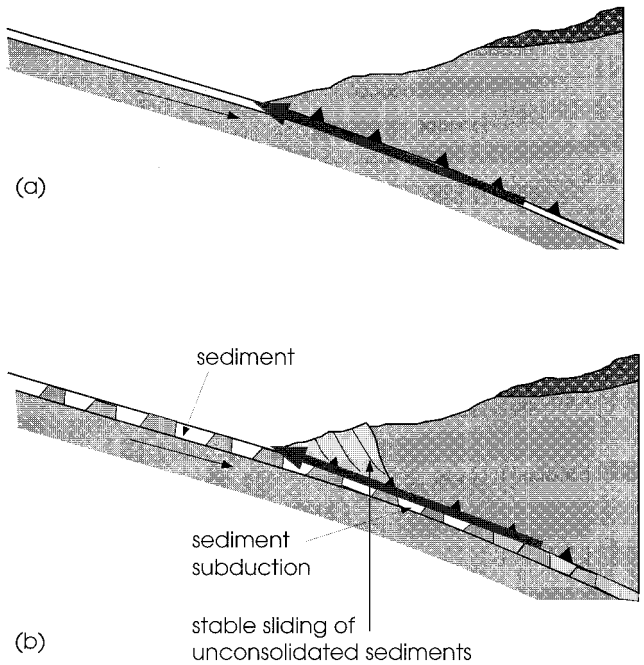

Figure 13. Models for (a) shallow earthquakes in sediment-starved subduction zones and (b) tsunami earthquakes with rough subducting ocean floor.

trench in these regions, the earthquake can breach the surface and generate great tsunamis. Although a large amount of slip at shallow depths at the plate interface occurred during the Nicaragua main shock, very few aftershocks are located in this region (Ihmle 1996; Piatanesi *et al.* 1996). This suggests that although the rupture could propagate through this area, there is no or little nucleation of events possible in this region, similar to conditionally stable friction behaviour. This may be because, in the shallowest part of the subduction zone, a thin layer of sediments still covers the top of the horsts, which would possibly support the propagation of a rupture, but will not nucleate earthquakes, and will also enhance the smoothness of the rupture. This thin layer may be scraped o and deposited in the grabens further down the trench or may quickly be compressed or dehydrated.

The presence of sediments in the rupture zone also explains the slow character of these tsunami events. This is only possible in regions where the sediment transport is not so great as to cover the horsts with a thick layer of sediments, which would completely remove the contact zone with the overriding plate. Also, if the accretionary prism were large, the earthquake would not be able to break through to the surface. Of course, in the case of a large accretionary prism there would be the risk of massive slumping, which would also generate a great tsunami. Since these slow tsunami earthquakes are really exceptional events, in a part of the subduction zone where usually no earthquakes can propagate, there will be few shallow thrusting aftershocks, and normal faulting events in the outer rise, in the overriding or subducting plate or in the accretionary prism will dominate the aftershock sequence. If we assume that the seismic slip of these earthquakes starts further down-dip but is much smaller in amplitude than the shallower slip close to the trench, this would also explain the aftershock zones being larger than the area of concentrated slip close to the trench needed by tsunami modellers (Satake & Tanioka 1999).

This model explains many of the seismic and tectonic signatures of slow tsunami earthquakes that were mentioned at the start of this section. However, it does not explain why the tsunamis caused by these events, for example the Nicaragua earthquake, are often found by tsunami modellers to be underestimated by their seismic moment (Imamura *et al.* 1993; Satake 1994), whereas other shallow earthquakes such as the event near Jalisco produce tsunamis seemingly more consistent with their moment magnitude. We suggest that the sea-bottom displacement calculated from the seismic moment for these slow events might be underestimated. In the process of determining moment from seismic amplitudes and subsequently determining displacement from this moment, the soft sedimentary structure in the fault zone of these earthquakes may not be (correctly) taken into account. In the conventional seismic source inversion method, a source structure with a simple laterally uniform crust without thick sediments is used. Tsunami modellers may thus underestimate the tsunami caused by a slow tsunami earthquake because the displacement calculated from the seismic moment using a standard rigidity model is not representative of the true ocean floor deformation (Satake 1995). Although it is di cult to treat this problem rigorously, we can illustrate this situation by the simplified cartoon shown in Fig. 14. For all three panels in this cartoon the observed displacement at the observing station has the same value, u_0. In the two left-hand side cases the model is a homogenous half-space with di erent rigidities but identical sources. Since displacement is proportional to source moment over rigidity, the rigidity drops out of the equation and the two displacements at the station are the same. In this simplified case, the moment determined from this displacement would be the same if the same standard reference model was used in the computation. However, the true 'source moment' is di erent, although the source displacements (the determining factor for tsunami generation) are in fact identical. In the rightmost case the model consists of two di erent rigidities adjacent to each other. Here, if the displacement at the station is u_0, the true displacement at the source in material with rigidity μ_2 is $D_T = D_1(\mu_1/\mu_2)$, which is larger than D_1 if the source material is of lower rigidity than the receiver-side rigidity. Alternatively, if we put in the same source as in the two panels to the left, with displacement D_1 and area A_0, the measured displacement at the surface will be smaller than u_0. Thus, if this observed displacement at the station is translated into a moment using the same standard reference model, it will underestimate the source displacement.

The actual depth of the slip is another important factor in the e ciency of tsunami generation. Although a simple dislocation model of a shallow thrust fault produces similar or even somewhat greater vertical displacements for a buried fault (slip stops at 5 km depth) as for a fault that reaches the surface, the horizontal displacement for the latter is four times greater than the horizontal displacement of the buried fault, which is of the same order as the vertical displacement. The wavelengths of the deformation are comparable for both cases. Since the topography in the trench region is pronounced, horizontal displacement of the ocean floor should still be an important factor in the excitation of tsunami waves (Satake & Kanamori 1990).

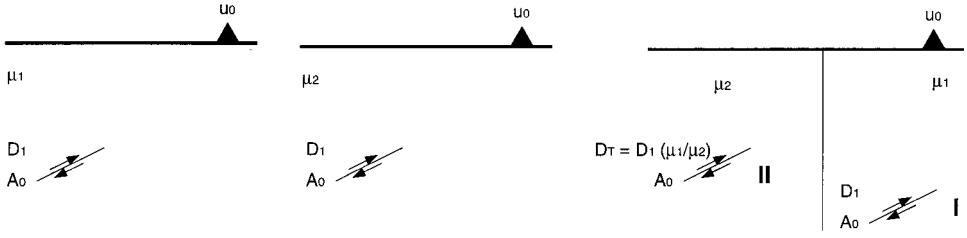

Figure 14. Simplified cartoon of the e ect of rigidity variations on calculated moment. (a), (b) Identical sources in di erent homogenous rigidity models produce the same displacement at the station, which would result in the same moment being determined for both, although their 'source moments' are di erent. (c) In this inhomogeneous rigidity model, source I will produce the same displacement at the receiver as source II. However, if μ_2 is smaller than μ_1, the true displacement of source II is larger than that of source I.

CONCLUSIONS

We have examined the source spectra of all recent large shallow subduction zone earthquakes. From the moment rate values calculated from teleseismic *P* waves for the 1992 Nicaragua and Java earthquakes as well as the 1996 event o shore Peru, we demonstrated that these events released relatively little energy in the high frequencies with respect to their seismic moment. These three earthquakes also caused tsunamis greater than would be expected from their moment, and can thus be called 'tsunami earthquakes'. Other earthquakes in this data set that were followed by great tsunamis either did not cause them directly (the Flores Island tsunami was most likely caused by a triggered landslide, the New Guinea one by a sediment slump) or did not cause disproportionately great tsunamis (the 1994 Kuril Island event). Therefore, we classify the Java, Nicaragua and Peru events as slow tsunami earthquakes, a subclass of tsunami earthquakes, for which the e ciency of tsunami excitation is directly related to the earthquake source process itself.

Examination of the centroid locations and epicentres of all these events showed that almost all ruptured up-dip and that the three slow tsunami events ruptured unusually close to the trench axis, possibly even to the ocean floor itself. Ocean floor survey results suggest that in all three regions the ocean floor close to the trench is highly faulted, there exists only a small accretionary prism and a thin layer of sediments is being subducted.

Most earthquakes examined seem to conform to the simple model of shallow subduction thrust faulting: the rupture is initiated in the unstable friction regime, where the sediments have been dehydrated and compacted, and ruptures up-dip, where its propagation is stopped by the stable region of unconsolidated sediments. In the case of sediment-starved subduction zones, it is possible for the earthquake to rupture all the way to the surface (and also to be nucleated at shallower depths). In the case of tsunami earthquakes, the rough surface of the subducting ocean floor (the horsts) makes contact with the overriding plate. Sediments are subducted in the grabens. This makes it possible for the earthquake to nucleate at a shallow depth and propagate up to the trench. These earthquakes will propagate through sediments, making the rupture process slow. The amount of sediment being subducted and that being scraped o to form the accretionary prism has to be relatively small for this model to work. If a large accretionary prism is formed, the stable sliding part of the shallow subduction zone might be too great for the earthquake to be able to break through to the surface, and in the case of a thick layer of subducting sediments, the horst structures might be completely covered, so that there are no contact zones with the overriding plate.

We suggest that the relatively great tsunami excitations with respect to their moments of these slow tsunami earthquakes can be explained by two factors. First, because the slip occurs at shallow depth, the water displacement will be relatively great. Second, these earthquakes may excite greater tsunamis than earthquakes with the same moment and slip distribution with depth in sediment-starved trenches because the moment as determined with a standard model for the elastic parameters does not represent and underestimates the true displacement of the ocean floor because of the sediment-rich source region of the event.

ACKNOWLEDGMENTS

We would like to thank Dr Emil Okal, an anonymous reviewer and Dr Steven Ward for their helpful comments and suggestions for improvements. This research was partially supported by US Geological Survey grant 99HQGR0035 and NSF grant EAR-9909352. Contribution #8667, Division of Geological and Planetary Sciences, California Institute of Technology.

REFERENCES

Bilek, S.L. & Lay, T., 1999. Comparison of depth dependent fault zone properties in the Japan trench and Middle America trench, *Pure appl Geophys.,* **154,** 433–456.

Boore, D.M. & Boatwright, J., 1984. Average body-wave radiation coe cients, *Bull. seism. Soc. Am.,* **74,** 1615–1621.

Bourgeois, J. *et al.,* 1999. Geologic setting, field survey and modeling of the Chimbote, northern Peru, tsunami of 21 February 1996, *Pure appl Geophys.,* **154,** 513–540.

Byrne, D.E., Davis, D.M. & Sykes, L.R., 1988. Loci and maximum size of thrust earthquakes and the mechanics of the shallow region of subduction zones, *Tectonics,* **7,** 833–857.

Dmowska, R., Zheng, G. & Rice, J.R., 1996. Seismicity and deformation at convergent margins due to heterogeneous coupling, *J. geophys. Res.,* **101,** 3015–3029.

Engdahl, E.R., van der Hilst, R. & Buland, R., 1998. Global teleseismic earthquake relocation with improved travel times and procedures for depth determination, *Bull. seism. Soc. Am.,* **88,** 722–743.

Fukao, Y., 1979. Tsunami earthquakes and subduction processes in island arcs, *J. geophys. Res.,* **84,** 2303–2314.

Hartog, J.R. & Schwartz, S.Y., 1996. Directivity analysis of the December 18, 1994 Sanriku-Oki earthquake (Mw = 7.7), Japan, *Geophys. Res. Lett.,* **23,** 2037–2040.

Hidayat, D., Barker, J.S. & Satake, K., 1995. Modeling the seismic source and tsunami generation of the December 12 1992, Flores island, Indonesia, earthquake, *Pure appl. Geophys.,* **144,** 537–554.

Hilde, T.W.C., 1983. Sediment subduction versus accretion around the Pacific, *Tectonophys.,* **99,** 381–397.

Houston, H. & Kanamori, H., 1986. Source spectra of great earthquakes, *Bull. seism. Soc. Am.,* **76,** 119–142.

Hyndman, R.D., Yamano, M. & Oleskevich, D.A., 1997. The seismogenic zone of subduction thrust faults, *Island Arc,* **6,** 244–260.

Ide, S., Imamura, F., Yoshida, Y. & Abe, K., 1993. Source characteristics of the Nicaraguan tsunami earthquake of September 2, 1992, *Geophys. Res. Lett.,* **20,** 863–866.

Ihmle, P.F., 1996. Frequency-dependent relocation of the 1992 Nicaragua slow earthquake, an empirical Greens-function approach, *Geophys. J. Int.,* **127,** 75–85.

Imamura, F., Shuto, N., Ide, S., Yoshida, Y. & Abe, K., 1993. Estimate of the tsunami source of the 1992 Nicaragua earthquake from tsunami data, *Geophys. Res. Lett.,* **20,** 863–866.

International Survey Team, 1997. *1996 Peruvian Tsunami,* http://www.geophys.washington.edu/tsunami/Peru/peru.html.

Kanamori, H., 1972. Mechanism of tsunami earthquakes, *Phys. Earth planet. Inter.,* **6,** 346–359.

Kanamori, H. & Kikuchi, M., 1993. The 1992 Nicaragua earthquake: a slow earthquake associated with subducted sediments, *Nature,* **361,** 714–716.

Kulm, L.D., Prince, R.A., French, W., Johnson, S. & Masias, A., 1981. Crustal structure and tectonics of the central Peru continental margin and trench, in *Nazca Plate: Crustal formation and Andean Convergence,* eds Kulm, L.D., Dymond, J., Dasch, E.J. & Hussong, D.M., *Geol. Soc. Am. Mem.,* **154,** 445–468.

Masson, D.G. *et al.,* 1990. Subduction of seamounts at the Java trench—a view with long-range sidescan sonar, *Tectonophysics,* **185,** 51–65.

Masson, D.G., Milsom, J. & Barber, A.J., 1991. Recent tectonics around the island of Timor, eastern Indonesia, *Mar. Petrol. Geol.,* **8,** 35–49.

Nakayama, W. & Takeo, M., 1997. Slip history of the 1994 Sanriku-Haruka-Oki, Japan, earthquake deduced from strong motion data, *Bull. seism. Soc. Am.,* **87,** 918–931.

Newman, A.V. & Okal, E.A., 1998. Teleseismic estimates of radiated seismic energy: the E/M-0 discriminant for tsunami earthquakes, *J. geophys. Res.,* **103,** 26 885–26 898.

Okal, E.A., 1988. Seismic parameters controlling far-field tsunami amplitudes: a review, *Nat. Hazards,* **1,** 67–96.

Pacheco, J. *et al.,* 1997. The October 9, 1995 Colima-Jalisco, Mexico earthquake (M-W 8): an aftershock study and a comparison of this earthquake with those of 1932, *Geophys. Res. Lett.,* **24,** 223–2226.

Piatanesi, A., Tinti, S. & Gavagni, I., 1996. The slip distribution of the 1992 Nicaragua earthquake from tsunami run-up data, *Geophys. Res. Lett.,* **23,** 37–40.

Satake, K., 1994. Mechanism of the 1992 Nicaragua tsunami earthquake, *Geophys. Res. Let.,* **21,** 2519–2522.

Satake, K., 1995. Linear and nonlinear computations of the 1992 Nicaragua earthquake tsunami, *Pure appl. Geophys.,* **144,** 455–470.

Satake, K. & Kanamori, H., 1990. Fault parameters and tsunami generation of the May 23, 1989, MacQuarie ridge earthquake, *Geophys. Res. Lett.,* **17,** 997–1000.

Satake, K. & Tanioka, Y., 1999. Sources of tsunami and tsunamigenic earthquakes in subduction zones, *Pure appl. Geophys.,* **154,** 467–483.

Sato, T., Imanishi, K. & Kosuga, M., 1996. 3-stage rupture process of the 28 December 1994 Sanriku-Oki earthquake, *Geophys. Res. Lett.,* **23,** 33–36.

Scholz, C.H., 1998. Earthquakes and friction laws, *Nature,* **391,** 37–42.

Smith, W.H.F. & Sandwell, D.T., 1997. Global sea-floor topography from satellite altimetry and ship depth soundings, *Science,* **277,** 1956–62.

Synolakis, C.E. *et al.,* 1995. Damage conditions of East Java tsunamis of 1994 analyzed, *EOS, Trans. Am. geophys. Un.,* **76,** 261–262.

Tanioka, Y., Ru , L. & Satake, K., 1996. The Sanriku-Oki, Japan, earthquake of December 28, 1994 (Mw = 7.7)—rupture of a di erent asperity from a previous earthquake, *Geophys. Res. Lett.,* **23,** 1465–1468.

Tanioka, Y., Ru , L. & Satake, K., 1997. What controls the lateral variation of large earthquake occurrence along the Japan trench, *Island Arc,* **6,** 261–266.

Taylor, M.A.J., Zheng, G., Rice, J.R., Stuart, W.D. & Dmowska, R., 1996. Cyclic stressing and seismicity at strong coupled subduction zones, *J. geophys. Res.,* **101,** 8363–8381.

Tappin, D.R. *et al.,* 1999. Sediment slump likely caused 1998 Papua New Guinea tsunami, *EOS, Trans. Am. geophys. Un.,* **80,** 329, 334, 340.

Tsuji, Y., Matsutomi, H., Imamura, F., Takeo, M., Kawata, Y., Matsuyama, M., Takahashi, T. & Sunarjo Harjadi, P., 1995. Damage to coastal villages due to the 1992 Flores island earthquake tsunami, *Pure appl. Geophys.,* **144,** 481–524.

von Huene, R. & Scholl, D.W., 1991. Observations at convergent margins concerning sediment subduction, subduction erosion, and the growth of continental crust, *Rev. Geophys.,* **29,** 279–316.

von Huene, R., Pecher, I.A. & Gutscher, M.A., 1996. Development of the accretionary prism along Peru and material flux after subduction of Nazca Ridge, *Tectonics,* **15,** 19–33.

von Huene, R., Weinrebe, W., Ranero, C., Heeren, F., Walther, C. & Stehr, G., 1998. PACOMAR 3, http://www.geomar.de/sci_dpmt/geodyn/d_so107_pac.html.

Walther, Ch.H.E. & Flueh, E.R., 1998. From Cocos to Carribean plate—geophysical investigations at the Pacific coast of Nicaragua, *EGS Abstr. Vol.,* **16,** 287.

Wang, C.Y. & Mao, N.H., 1979. The mechanical property of montmorillonite clay at high pressure and implications on fault behavior, *Geophys. Res. Lett.,* **6,** 476–478.

Ward, S.N., 1982. On tsunami nucleation 2. An instantaneous modulated line source, *Phys. Earth planet. Inter.,* **27,** 273–285.

APPENDIX A: SOURCE SPECTRA FOR ALL EVENTS IN TABLE 1

Annotations are as in Fig. 2(b).

1992 5 15 7 5 2 EASTERN NEW GUINEA REG., P.N.G.

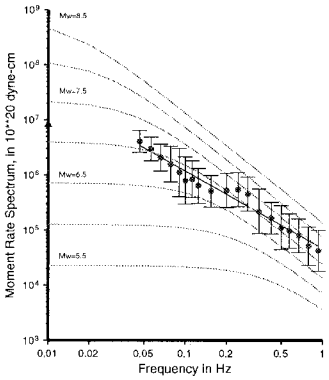

1992 9 2 0 16 0 NEAR COAST OF NICARAGUA

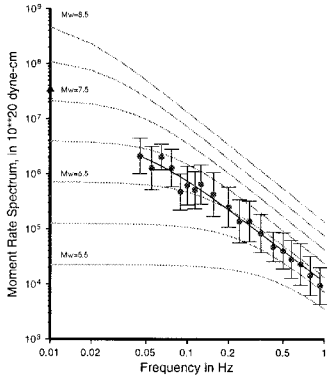

1992 10 18 15 12 1 NEAR WEST COAST OF COLOMBIA

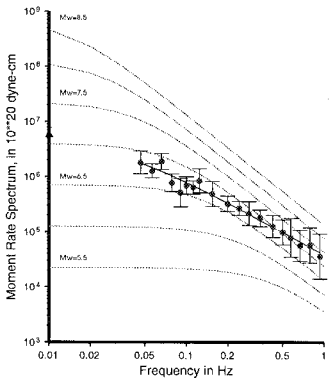

1992 12 12 5 29 27 FLORES REGION, INDONESIA

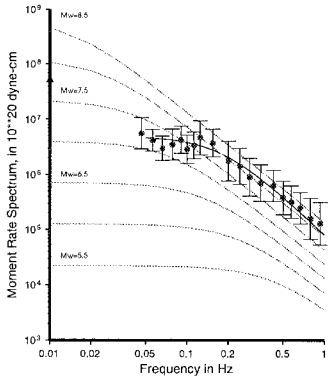

1993 6 8 13 3 32 NEAR EAST COAST OF KAMCHATKA

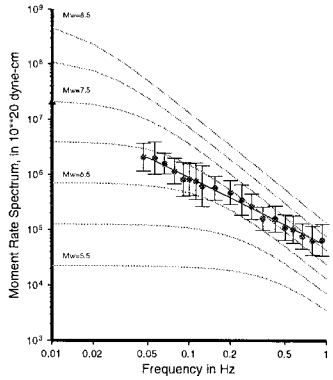

1993 7 12 13 17 15 EASTERN SEA OF JAPAN

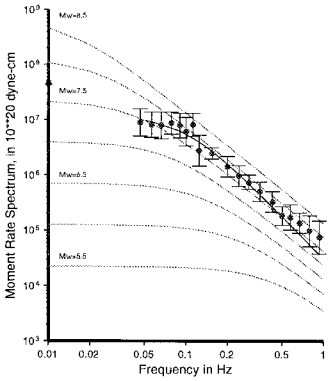

1993 9 10 19 12 54 NEAR COAST OF CHIAPAS, MEXICO

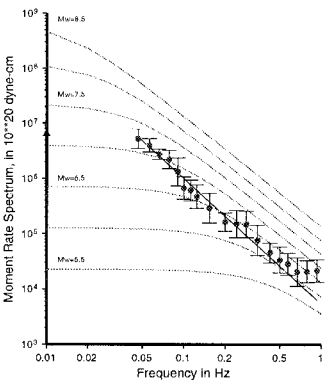

1994 6 2 18 17 37 SOUTH OF JAWA, INDONESIA

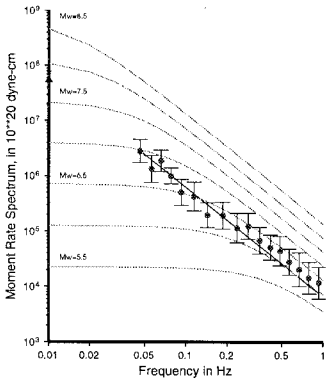

1994 10 4 13 22 58 KURIL ISLANDS

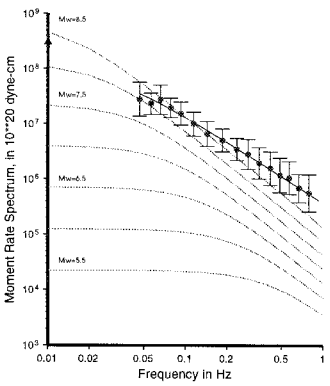

1994 10 9 7 55 39 EAST OF KURIL ISLANDS

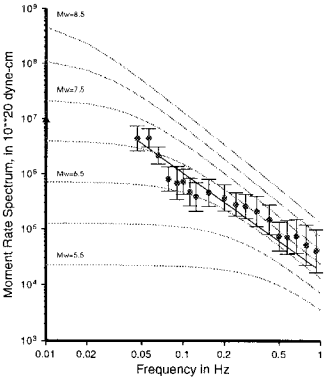

1994 12 28 12 19 24 OFF EAST COAST OF HONSHU, JAPAN

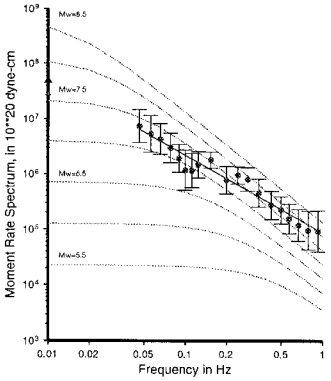

1995 2 5 22 51 7 OFF E. COAST OF N. ISLAND, N.Z.

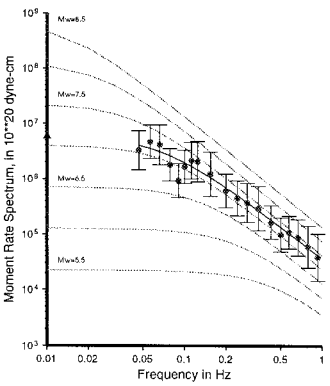

1995 5 5 3 53 46 SAMAR, PHILIPPINE ISLAND

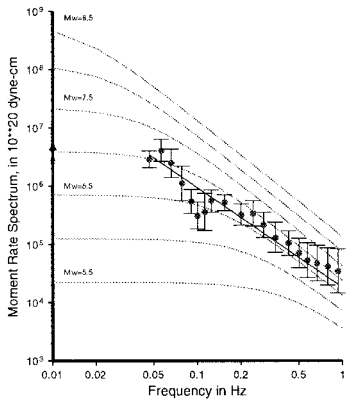

1995 5 16 20 12 45 LOYALTY ISLANDS REGION

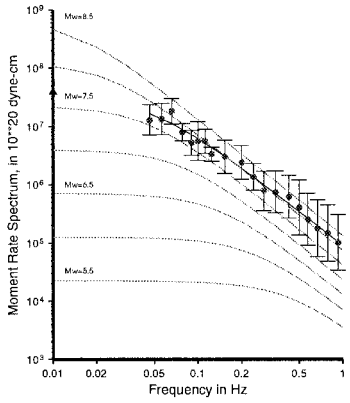

1995 7 3 19 50 50 KERMADEC ISLANDS, NEW ZEALAND

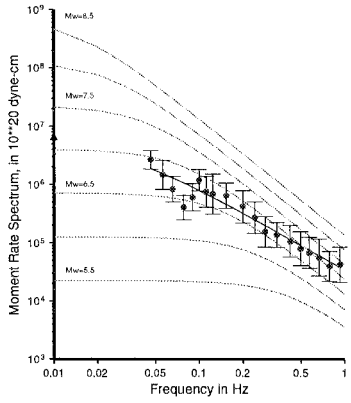

1995 7 30 5 11 21 NEAR COAST OF NORTHERN CHILE

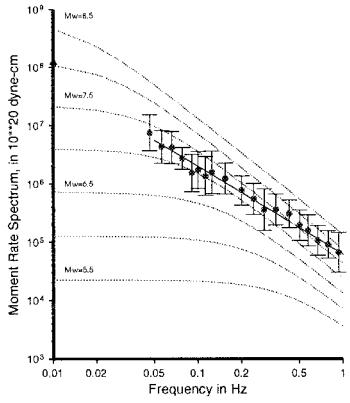

1995 8 16 10 27 28 SOLOMON ISLANDS

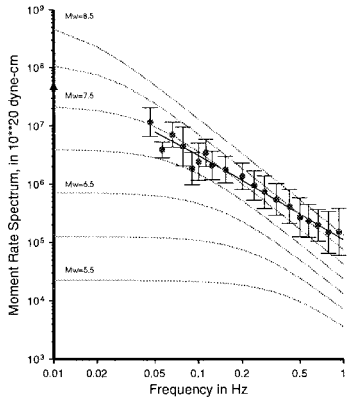

1995 8 16 23 10 27 SOLOMON ISLANDS

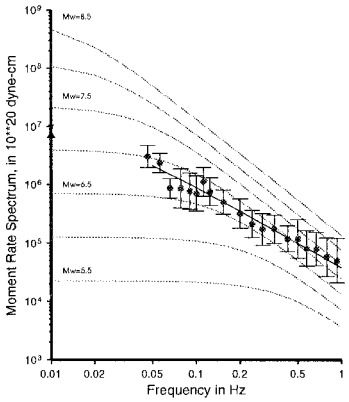

1995 9 14 14 4 31 NEAR COAST OF GUERRERO

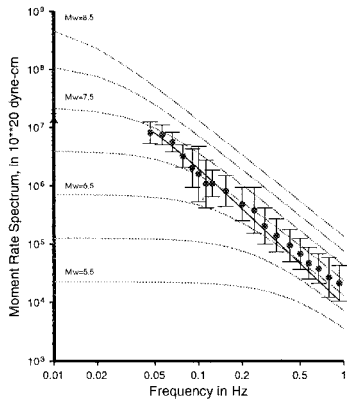

1995 10 9 15 35 51 NEAR COAST OF JALISCO, MEXICO

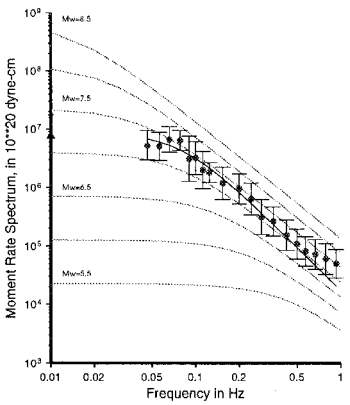

1995 10 18 10 37 26 RYUKYU ISLANDS

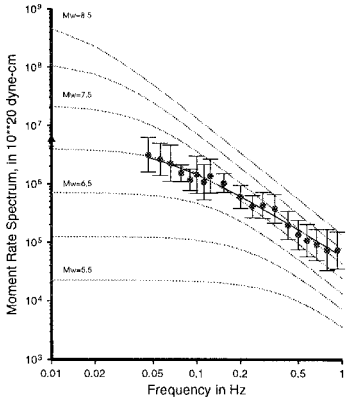

1995 12 3 18 1 9 KURIL ISLANDS

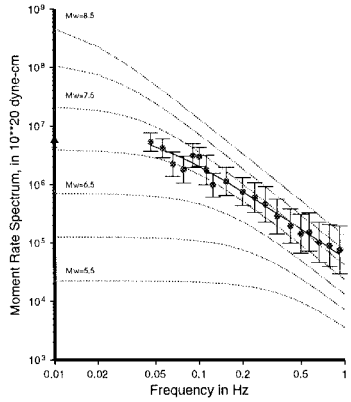

1996 1 1 8 5 11 MINAHASSA PENINSULA, SULAWESI

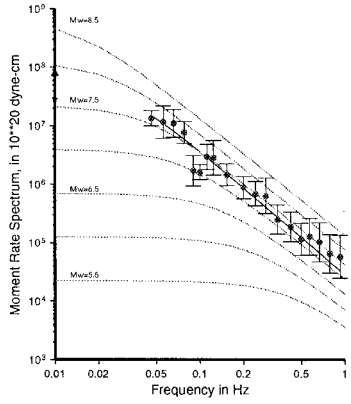

1996 2 7 21 36 44 KURIL ISLANDS

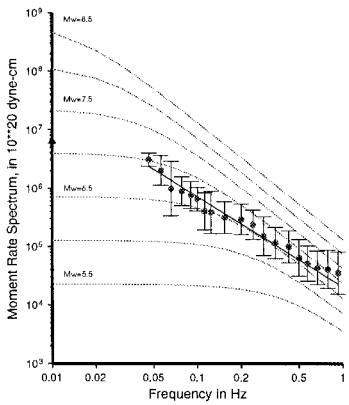

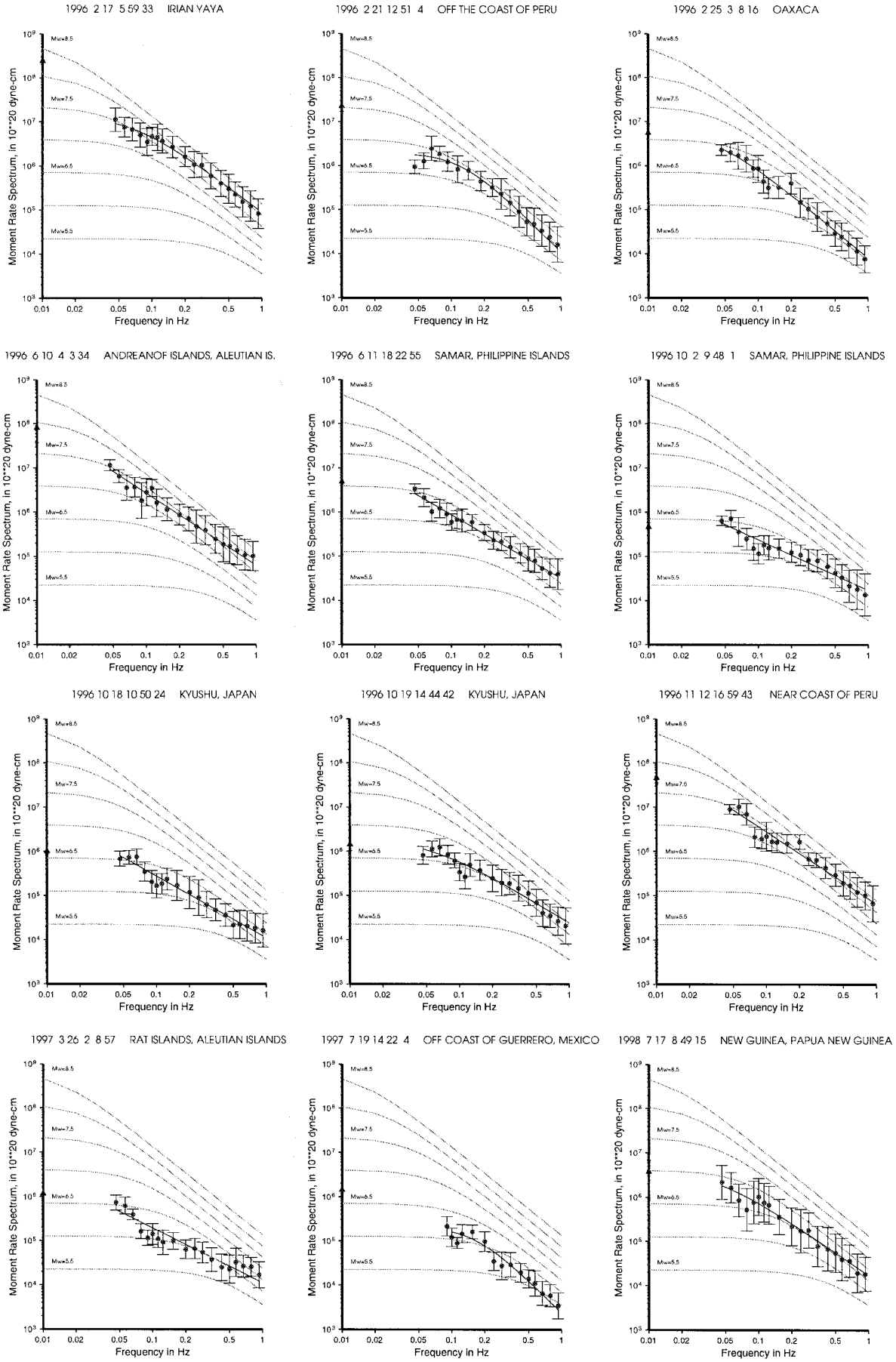
1996 2 17 5 59 33 IRIAN YAYA
1996 2 21 12 51 4 OFF THE COAST OF PERU
1996 2 25 3 8 16 OAXACA
1996 6 10 4 3 34 ANDREANOF ISLANDS, ALEUTIAN IS.
1996 6 11 18 22 55 SAMAR, PHILIPPINE ISLANDS
1996 10 2 9 48 1 SAMAR, PHILIPPINE ISLANDS
1996 10 18 10 50 24 KYUSHU, JAPAN
1996 10 19 14 44 42 KYUSHU, JAPAN
1996 11 12 16 59 43 NEAR COAST OF PERU
1997 3 26 2 8 57 RAT ISLANDS, ALEUTIAN ISLANDS
1997 7 19 14 22 4 OFF COAST OF GUERRERO, MEXICO
1998 7 17 8 49 15 NEW GUINEA, PAPUA NEW GUINEA
Moment Rate Spectrum, in 10**20 dyne-cm
Frequency in Hz
Mw=8.5
Mw=7.5
Mw=6.5
Mw=5.5